Experimental investigation of wall temperature variation caused by internal heat generation in a vertical pipe flow for molten salt reactor applications

Dong-Hyuk Park and Bum-Jin Chung
Department of Nuclear Engineering, Kyung Hee University
#1732 Deogyeong-daero, Giheung-gu, Yongin-si, Gyeonggi-do, 17104, Korea
Corresponding author: bjchung@khu.ac.kr

***Keywords : Molten salt reactor; Internal heat generation; buoyancy effect**

1. Introduction

Molten Salt Reactors (MSRs) are considered promising Generation IV nuclear systems due to their low-pressure operation, high thermal efficiency, and inherent safety characteristics [1]. In liquid-fueled MSRs, the nuclear fuel is dissolved directly in the coolant, leading to volumetric heat generation within the fluid rather than surface heating from solid fuel rods. This internal heat generation (IHG) occurs not only in the core but also in out-of-core components due to decay heat, resulting in continuous wall temperature rise along the flow path [2].

Therefore, accurate prediction of wall temperature under IHG conditions is essential for MSRs operating at high temperatures, where additional temperature rise may reduce structural material margins and accelerate corrosion. However, conventional wall-heating heat transfer models can not directly applicable because IHG introduces a volumetric source term in the energy equation, fundamentally altering the thermal-hydraulic behavior.

For this reason, several studies related to IHG have been proposed [3-9]. However, experimental investigations have remained scarce since the 1970s [10, 11]. Most recent studies have relied primarily on numerical analyses, with experimental efforts largely confined to conceptual or planning stages [7].

In this study, wall temperature variations induced by IHG were experimentally examined in laminar pipe flow under adiabatic wall conditions. Uniform IHG was generated using high-frequency alternating current applied to an electrolyte solution. This study provides new experimental data for IHG flows relevant to MSRs thermal-hydraulic design and safety evaluation.

2. Experimental setup

2.1 Experimental apparatus

Figure 1 presents a photograph of the experimental loop. The working fluid, a sulfuric acid solution, was continuously circulated through the loop using a pump. The fluid flowed sequentially through a flowmeter, an entrance section, the test section, and a downstream mixing section before finally returning to the reservoir. The test section was arranged in an upward flow configuration so that the buoyancy force induced by IHG acts in the same direction as the main flow.

Due to the corrosive nature of the sulfuric acid solution, the flow loop was constructed using non-metallic pipes made of polyvinyl chloride (PVC). A straight entrance section with a length of 1.0 m was installed upstream of the test section to ensure a hydrodynamically fully developed inlet flow. Downstream of the test section, a mixing section equipped with orifice plates was employed to homogenize the outlet fluid temperature. Two K-type thermocouples were installed in the entrance section to measure the inlet temperature, while three thermocouples were located downstream of the mixing section to measure the bulk outlet temperature. To maintain a stable inlet temperature during the experiments, a copper heat exchanger was installed within the fluid reservoir.

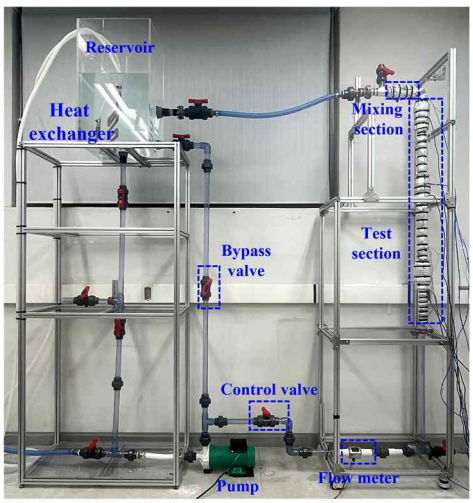

Fig. 1. Experimental loop for forced convection with internal heat generation.

Uniform volumetric heat generation was achieved via electrical Joule dissipation within an electrolyte solution. To prevent electrochemical reactions such as electrolysis at the electrodes, a 260 Hz alternating current was applied across the working fluid. This frequency ensured that the supplied electrical energy was converted almost entirely into thermal energy within the bulk fluid. Ring-shaped graphite electrodes were installed to maintain

stable electrical contact. Power was supplied from a single-phase 220 V (60 Hz) to a variable autotransformer, whose output was converted to a 260 Hz signal using a variable frequency drive inverter.

To measure the wall temperature distribution along the test section, eighteen K-type thermocouples were installed at nine equally spaced axial stations. At each station, two thermocouples were mounted at diametrically opposite positions. The entire test section was wrapped with fiberglass insulation to ensure adiabatic conditions by minimizing heat loss to the surroundings.

All experimental data, including current, voltage, and temperature, were acquired using a National Instruments (NI) data acquisition (DAQ) system. Temperature signals were recorded via NI-9212 modules. Electrical current and voltage were measured using NI-9247 and NI-9225 modules, respectively, ensuring precise and synchronized data logging.

2.2 Data processing

The average volumetric heat generation rate (Q) was calculated using the measured current and voltage as follows:

$$Q = \frac{\int_{t_1}^{t_2} V(t)I(t)dt}{(t_2 - t_1)\pi r_0^2 L}. \quad (1)$$

where L and r_o are the length and radius of the test section, respectively. According to the energy conservation law, the local bulk fluid temperature at location x, $T_b(x)$, was calculated as follows:

$$Q\pi r_0^2 x = \pi r_0^2 \rho c_p u_m (T_b(x) - T_i) \text{ and} \quad (2)$$

$$T_b(x) = \frac{Qx}{\rho c_p u_m} + T_i. \quad (3)$$

For IHG flow, the non-dimensional wall-to-bulk fluid temperature difference, which is denoted as Θ in this study, is expressed as follows:

$$\Theta = \frac{k(T_w - T_b)}{Qr_0^2}. \quad (4)$$

Θ is analogous to the inverse of the Nu in wall heated heat transfer. This relationship becomes evident when the denominator is rewritten as Qr_0/k.

To represent the buoyancy effect in IHG flow, the modified Grashof number (Gr^*) was calculated as follows [12]:

$$Gr^* = \frac{g\beta\Delta T D^3}{\nu^2}\frac{QD^2}{k\Delta T} = \frac{g\beta Q D^5}{\nu^2 k}. \quad (5)$$

The non-dimensional axial distance (X^+) was calculated as Eq. (6). This parameter is widely used in forced convection laminar heat transfer and represents the growth of the thermal boundary layer along the flow direction [13].

$$X^+ = \frac{x/D}{RePr}. \quad (6)$$

2.3 Test matrix

Table 1 shows the test matrix for present study. The test section had a fixed inner diameter of 0.02 m and a heated length of 1.05 m. The Prandtl number (Pr) ranged from 8.28 to 9.06 and the Reynolds number (Re) ranged from 210 to 950. The volumetric heat generation rate (Q) was adjusted between 0.35–3.47 MW/m^3 by varying the concentration of sulfuric acid and the applied voltage. The corresponding Gr^* ranged from 1.16×10^6 to 2.07×10^7.

Table 1. Test matrix.

Pr	Q (MW/m^3)	Gr^*	Re
8.28–9.06	0.35	1.16×10^6	210–940
	0.61	2.33×10^6	
	0.90	3.30×10^6	
	1.37	5.49×10^6	
	1.72	7.44×10^6	
	2.01	1.06×10^7	360–950
	2.81	1.55×10^7	
	3.47	2.07×10^7	

3. Results and discussion

3.1 Data validation

Figure 2 shows a comparison between the axial non-dimensional wall-to-bulk temperature distribution (Θ) obtained in the present experiments and the laminar analytical results of Sparrow and Siegel with assumption of pure forced convection [14]. The symbols represent the experimental data for the lowest heat generation case (Q = 0.35 MW/m^3).

Because the fluid velocity near the wall is lower than in the core region due to wall friction, the local residence time increases. Since IHG occurs uniformly within the fluid, the increased residence time near the wall, results in higher wall temperature than the bulk fluid

temperature, yielding a positive Θ that increases with axial position X^+.

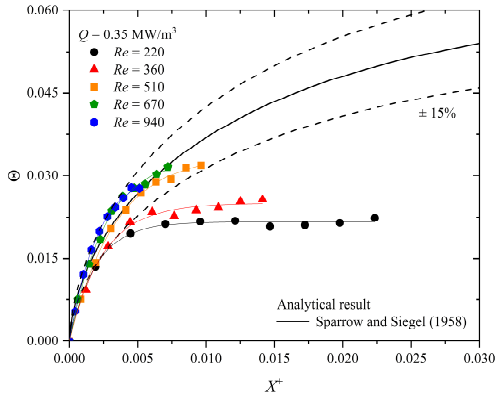

Fig. 2. Comparison of the axial distributions of Θ in the present experiments at the lowest heat generation rates with analytical results for pure forced convection.

For *Re*'s exceeding 510, the experimental data matched well with the analytical prediction falling well within the ±15% deviation limits. However, for the lower *Re* cases (*Re* = 220 and 360), Θ progressively deviates from the analytical curve as X^+ increases. This deviation is attributed to the relative buoyancy effect which is not considered in analytical model.

As *Re* decreases, the temperature rise caused by IHG becomes larger, leading to a larger wall-to-bulk temperature difference. When this temperature difference becomes sufficiently large, buoyancy force cannot be neglected. Consequently, Θ values become lower than the pure forced convection analytical results.

Nevertheless, the fact that the high *Re* cases closely align with the pure forced convection analytical results demonstrate that the present experimental system successfully achieves a nearly uniform volumetric heat source, since any significant nonuniformity in heat generation would have caused deviations, even in the forced convection dominated regime.

3.2 Influence of buoyancy on wall temperature distribution in IHG flow

As discussed above, the pure forced convection behavior is observed only when the wall-to-bulk temperature difference caused by IHG is sufficiently small. When the heat generation rate is high or the mass flow rate is relatively low, a substantial radial temperature difference develops, which in turn induces significant buoyancy force as shown in Fig. 3.

Since the fluid near the wall is hotter than the core fluid, the upward buoyancy force acts in the same direction as the main flow. This buoyancy force locally accelerates the fluid near the wall. To satisfy mass conservation, this near-wall acceleration must be accompanied by a deceleration of the fluid in the core region resulting in a flattened velocity profile. As the flow develops further, or as buoyancy effects intensify, the velocity profile can transform into an M-shaped profile [5].

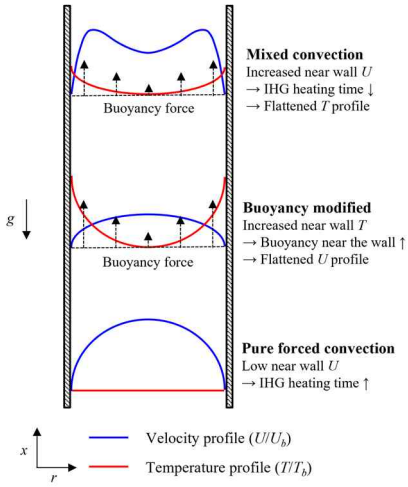

Fig. 3. Schematic illustration of the development of buoyancy affected velocity and temperature profiles in an adiabatic vertical pipe flow with internal heat generation.

Due to these flattened or M-shaped velocity profiles, the difference in residence time between the near-wall and core regions is significantly reduced compared to the parabolic case. The increased near-wall velocity reduces the local heating time, relaxing the temperature rise at the wall. As a result, Θ becomes lower than the analytical prediction from pure forced convection, as shown in red and black symbols in Fig. 2.

3.3 Influence of volumetric heat generation magnitude and Reynolds number

Figure 4 shows the influence of the volumetric heat generation magnitude (*Q*) on the axial profiles of Θ. As *Q* increases, the overall magnitude of Θ decreases. This is because the larger wall-to-bulk temperature difference induced by high *Q* enhances buoyancy force near the wall.

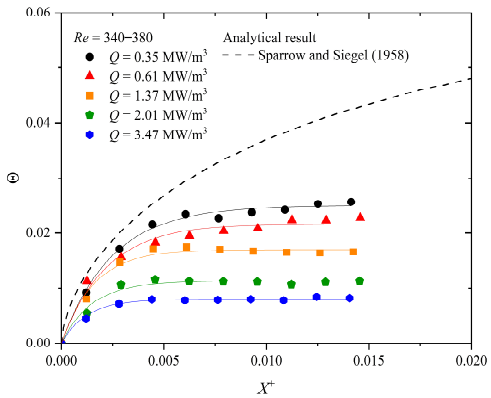

Fig. 4. Influence of *Q* on non-dimensional temperature difference at *Re* = 340–380.

Figure 5 shows the influence of *Re* on the axial profiles of Θ. It should be noted that, as *Re* increases, the same axial location x/D corresponds to a smaller X^+, resulting in a decrease in the range of X^+ with increasing *Re*.

At lower *Re*, the increased residence time leads to a larger dimensional wall-to-bulk temperature difference. This substantial temperature gradient intensifies the buoyancy force near the wall. This buoyancy force accelerates the near-wall fluid, flattening the velocity profile and resulting in a lower Θ compared to the pure forced convection prediction.

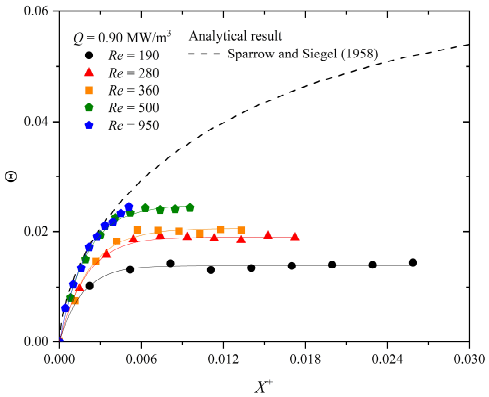

Fig. 5. Influence of *Re* on non-dimensional temperature difference at $Q = 0.90$ MW/m^3.

3.4 Buoyancy coefficient for vertical mixed convection IHG flow

Buoyancy effects depend on both *Q* and *Re*. To account for buoyancy effect in IHG flows, it is necessary to identify an appropriate buoyancy parameter. For the dimensionless number representing the volumetric heat generation rate, *Gr** is denoted as defined in Eq. (5).

Buoyancy parameters (*Bo*) are generally derived from the ratio of the three dominant forces appearing in the momentum equation: inertial, viscous, and buoyancy forces. The first buoyancy coefficient (Bo_1), denoted in Eq. (7), represents the ratio of buoyancy to inertial forces. Second buoyancy coefficient (Bo_2), denoted in Eq. (8) represents the ratio of buoyancy to viscous force.

$$Bo_1 \sim \frac{g\beta\Delta T}{u\left(\partial u/\partial x\right)} \sim \frac{g\beta(QD^2/k)}{u^2/D} = \frac{Gr^*}{Re^2} \qquad (7)$$

$$Bo_2 \sim \frac{g\beta\Delta T}{\nu\left(\partial^2 u/\partial y^2\right)} \sim \frac{g\beta(QD^2/k)}{\nu u/D^2} = \frac{Gr^*}{Re} \qquad (8)$$

Figure 6 shows the relationship between Bo_1 and the wall temperature reduction ratio at thermally fully developed region, defined as Θ/Θ_{PFC}, where Θ_{PFC} is the value for pure forced convection which is equal to 0.0625 [13]. The results indicate that strong buoyancy force significantly reduces the wall temperature, with the ratio Θ/Θ_{PFC} decreasing to as low as 13%. Although Θ/Θ_{PFC} generally decreases as Bo_1 increases, the data exhibits significant scatter with respect to Gr^*. This deviation indicates that the inertial based scaling does not adequately capture the underlying physical behavior.

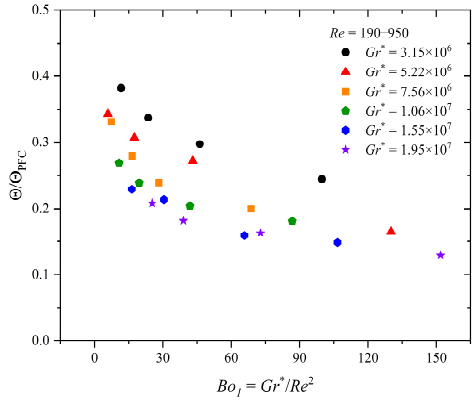

Fig. 6. Relationship between Bo_1 and the ratio of the measured dimensionless temperature (Θ) to the analytical pure forced convection value (Θ_{PFC}).

Figure 7 shows the relationship between Bo_2 and Θ/Θ_{PFC}. Unlike the previous case, Bo_2 provides a better collapse of the data points onto a single curve. This improvement arises from the fundamental difference between conventional wall heated systems and the internal heating system.

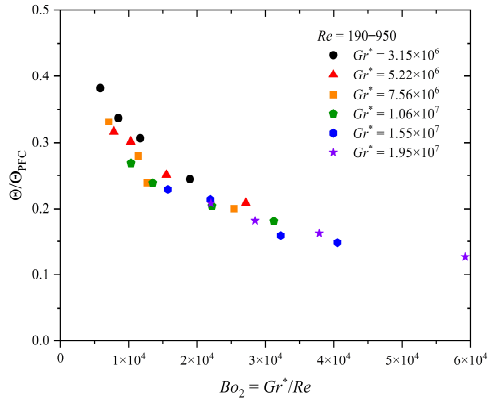

Fig. 7. Relationship between Bo_2 and the ratio of the measured dimensionless temperature (Θ) to the analytical pure forced convection value (Θ_{PFC}).

In conventional wall heated flows, the temperature field is governed primarily by the interaction between convection and thermal diffusion. Heat is supplied at the wall, and the wall temperature rises first, after which thermal diffusion transports energy toward the core. In this case, buoyancy competes mainly with the bulk inertial flow, and therefore Bo_1 is an appropriate parameter.

In contrast, for IHG flows, the temperature field is fundamentally controlled by viscous forces. Since the heat source is uniformly distributed within the fluid, the radial temperature gradient arises solely due to the variation in fluid residence time, which is established by the velocity profile. Physically, in the hypothetical

absence of viscosity, the flow would exhibit a plug profile where all fluid elements experience identical heating times, resulting in a uniform temperature distribution with no radial gradient. Consequently, in real IHG flows, the temperature nonuniformity is a direct result of viscous effects near the wall. Therefore, the dominant force balance lies between buoyancy and viscous forces.

3.5. Development of non-dimensional wall temperature correlations

It was confirmed that, the Bo_2 governs the present thermal hydraulic behaviors. Therefore, correlations for Θ were developed using Bo_2 as given in Eq. (9). When Bo_2 approaches zero, Θ_{fd} approaches the pure forced convection value of 0.0625. Eq. (9) was validated over the range $5.84\times10^3 < Bo_2 < 5.92\times10^4$ and predicted the experimental data well, with $R^2 = 0.948$, an average relative error of 3.83%.

$$\Theta_{fd} = \frac{0.0625}{(1+0.0116Bo_2^{0.580})}. \quad (9)$$

4. Conclusions

This study experimentally investigated buoyancy assisted wall temperature variations in laminar vertical pipe flow with internal heat generation under adiabatic conditions. Uniform volumetric heating up to 3.5 MW per cubic meter was achieved using high frequency alternating current applied to a sulfuric acid solution.

IHG intensified near wall heating due to viscous residence time effects. However, buoyancy induced acceleration near the wall mitigated excessive temperature rise, resulting in lower non dimensional wall temperatures compared with pure forced convection. The reduction became more significant at higher heat generation rates and lower Reynolds numbers.

Buoyancy parameter (Gr^*/Re) effectively characterizes the thermal behavior, and experimental correlations were developed to predict wall temperature variations under buoyancy assisted IHG conditions.

This work provides rare experimental data and a physically based predictive framework for IHG flows relevant to molten salt reactors. The results contribute directly to evaluating thermal margins and material integrity, particularly under reduced flow or natural circulation conditions, thereby supporting the safety analysis and design validation of MSRs systems.

5. Acknowledgements

This study was also sponsored by the Ministry of Science and ICT (MSIT) and was supported by nuclear Research & Development program grant funded by the National Research Foundation (NRF) (No. RS-2025-02653218).

REFERENCES

[1] J. Serp, M. Allibert, O. Beneš, S. Delpech, O. Feynberg, V. Ghetta, D. Heuer, D. Holcomb, V. Ignatiev, J.L. Kloosterman, L. Luzzi, E. Merle-Lucotte, J. Uhlíř, R. Yoshioka, D. Zhimin, The molten salt reactor (MSR) in generation IV: Overview and perspectives, Prog. Nucl. Energy, Vol. 77, p. 308–319, 2014.

[2] C. Fiorina, A. Cammi, L. Luzzi, K. Mikityuk, H. Ninokata, M.E. Ricotti, Thermal-hydraulics of internally heated molten salts and application to the Molten Salt Fast Reactor, in: Journal of Physics: Conference Series, IOP Publishing, p. 012030, 2014.

[3] Y. Yang, Y. Zou, Evaluation of the thermal hydraulic behavior of laminar developing fuel salt with combined internal heat generation and wall heat flux, Thermal Science and Engineering Progress, Vol. 63, 2025.

[4] D.-H. Park, B.-J. Chung, Influence of internal heat generation on heat transfer in an MSR heat exchanger under laminar flow condition, Nucl. Eng. Technol., Vol., p. 103736, 2025.

[5] Y. Yang, Y. Zou, Thermal-hydraulic and irreversibility analysis of laminar mixed convection of molten salt with internal heat source, Int. Commun. Heat Mass Transf., Vol. 167, 2025.

[6] D.-H. Park, B.-J. Chung, Experimental investigation of secondary flow effect caused by internal heat generation in the horizontal laminar pipe flow, Appl. Therm. Eng., Vol. 281, 2025.

[7] S. Wang, H. Deng, J. Tian, P. Huang, H. Yu, S. Xue, Y. Cao, C. Zhou, Y. Zou, Experimental Design and Numerical Analysis of Volume Internal Heat Generation Source in Fluids Based on Microwave Heating, Energies, Vol. 19(1), 2025.

[8] D.-H. Park, B.-J. Chung, Influence of internal heat generation on turbulent heat transfer in a pipe flow with wall cooling, Ann. Nucl. Energy, Vol. 226, 2026.

[9] H. Deng, C. Zhou, S. Wang, S. Xue, P. Huang, H. Yu, Flow and heat transfer characteristics in molten salt reactor core channels under the coupled influence of wall heat flux and volumetric internal heat generation, Ann. Nucl. Energy, Vol. 227, 2026.

[10] R.B. Kinney, E.M. Sparrow, Turbulent Pipe Flow of an Internally Heat Generating Fluid, J. Heat Transf., Vol. 88(3), p. 314–321, 1966.

[11] R.M. Inman, Experimental study of temperature distribution in laminar tube flow of a fluid with internal heat generation, Int. J. Heat Mass Transf., Vol. 5(11), p. 1053–1058, 1962.

[12] S.D. Lee, J.K. Lee, K.Y. Suh, Natural convection thermo fluid dynamics in a volumetrically heated rectangular pool, Nucl. Eng. Des., Vol. 237(5), p. 473–483, 2007.

[13] E.M. Sparrow, R. Siegel, Laminar Tube Flow with Arbitrary Internal Heat Sources and Wall Heat Transfer, Nucl. Sci. Eng., Vol. 4(2), p. 239–254, 1958.